Provably Stabilizing Controllers for Quadrupedal Robot Locomotion on Dynamic Rigid Platforms

Amir Iqbal [ID], Yuan Gao, and Yan Gu [ID]

Abstract—**Creating controllers for quadrupedal robot locomotion on platforms that exhibit dynamic behaviors, which are herein termed as dynamic platforms, poses a challenging problem because of the complexity of the associated hybrid, time-varying robot dynamics. Towards tackling this challenge, this article focuses on controller design for quadrupedal robot locomotion on dynamic rigid platforms, which are floating-base platforms with a rigid surface. The main contribution of this article is the derivation of a control approach that realizes stable quadrupedal robot locomotion on dynamic rigid platforms of known motions through the provable stabilization of the hybrid, time-varying robot control system. The control approach is synthesized based on the formulation of the robot model as a hybrid, time-varying system and the analysis of the closed-loop control system through the construction of multiple Lyapunov functions. Simulation and experimental results confirm the effectiveness of the proposed control approach in guaranteeing the stability and robustness of quadrupedal robot walking on dynamic rigid platforms.**

Index Terms—**Dynamic platforms, hybrid systems, legged locomotion, lyapunov methods, modeling, motion control.**

I. INTRODUCTION

QUADRUPEDAL robots have the potential to assist human operators in critical real-world applications such as emergency response and disaster relief [1], [2]. These applications may demand the capabilities of a quadrupedal robot in reliably traversing platforms that exhibit dynamic behaviors. Real-world examples of dynamic platforms include unstable buildings on disaster sites, vessels, and aircraft.

Controller design for quadrupedal robot locomotion on dynamic platforms poses a challenging problem due to the high complexity of the associated robot dynamics. Walking robot dynamics are inherently hybrid involving complex discrete behaviors [3]–[5] (i.e., uncontrolled sudden jumps in a robot's joint velocities when the swing foot strikes the platform surface).

Furthermore, the dynamics may become time-varying when the robot moves on dynamic platforms.

A. Related Work

Previous research on control design for legged robot locomotion has been mainly focused on static platforms, including flat and uneven terrains [6]–[12]. However, these approaches cannot reliably sustain stable legged locomotion on dynamic platforms, as demonstrated by the simulation results in this article, because such approaches do not explicitly account for the motion of the stance feet induced by the movement of the platform surface.

Control design for legged locomotion on dynamic platforms is an active research topic. Recently, locomotion on granular terrains, such as sand and gravels, has been increasingly intensively studied [13], [14]. Granular terrains are considered as dynamic platforms because the contact surface between a robot's stance foot and the terrain is subject to constant, and often significant, movements. Based on the previous modeling result, control approaches have been derived to enable impulsive robot hopping on granular terrains [15]. A stability criterion for planar bipedal robot walking on a granular terrain has been developed based on a general model of the leg-terrain interaction force [16], which can be used to guide the controller design for locomotion stabilization on granular terrains.

Besides granular terrains, floating-base platforms with a rigid surface, which are referred to as dynamic rigid platforms in this article, form another class of dynamic platforms that commonly exist in real-world environments, such as airplanes, vessels, and ground vehicles. Recently, control design for legged locomotion over dynamic rigid platforms has been increasingly researched [17], [18]. However, these control approaches only address the robot's continuous-phase dynamics but not the discrete foot-landing behaviors. The resulting model discrepancy may deteriorate the control performance, particularly when the landing impacts are significant during dynamic walking [7].

In addition to the hybrid nature, robot dynamics associated with locomotion over dynamic rigid platforms are also time-varying, due to the time-varying movement of the foot-platform contact points induced by the platform motion. To date, control design that explicitly addresses such hybrid, time-varying behaviors remains unsolved and underexplored.

Motivated by the current research needs, the objective of this article is to derive a control approach that provably realizes stable quadrupedal robot locomotion on dynamic rigid platforms

by explicitly addressing the associated hybrid, time-varying robot dynamics. We have previously introduced a model-based controller design for hybrid systems with state-triggered jumps that include legged robots walking on static platforms [19]. The controller explicitly addresses the robot's hybrid dynamics associated with static-terrain walking. Yet, the previous control approach is not directly applicable to legged locomotion on a dynamic platform, because it does not consider the time-varying global movement of the platform-robot contact points induced by the platform motion.

B. Contributions

The main contribution of this article is the derivation of a control approach that provably achieves stable quadrupedal robot locomotion on dynamic rigid platforms by explicitly addressing the associated hybrid, time-varying walking dynamics. As the initial step of our ongoing research on dynamic-platform locomotion, this article focuses on tackling the controller design challenge and assumes that the platform motion has been sensed or estimated.

The specific contributions of this article include the following.
1) Formulating the model of a quadrupedal robot that walks on a dynamic rigid surface as a hybrid, time-varying system with state-triggered jumps.
2) Extending our previous model-based control approach for static-terrain walking with the proposed system model to provably stabilize the hybrid, time-varying control system for realizing stable locomotion on dynamic rigid platforms.
3) Demonstrating through simulations that control laws synthesized for static-terrain walking may not guarantee stable locomotion on dynamic platforms.
4) Validating the effectiveness of the proposed control approach in guaranteeing the stability and robustness of locomotion on dynamic rigid platforms, both through simulations and experimentally on a physical quadrupedal robot.

The results of this article have not been previously reported. The rest of this article is organized as follows. Section II introduces the proposed full-order modeling of the hybrid, time-varying dynamics of a quadrupedal robot that walks on a dynamic platform, which serves as a basis of the proposed controller design. In Section III, a continuous control law is proposed to provably stabilize the closed-loop control system during continuous phases. The proposed Lyapunov-based stability analysis of the overall hybrid, time-varying system is introduced in Section IV. Section V presents the proposed model-based trajectory generation method. Simulation and experimental validation results are reported in Section VI. Discussions are given in Section VII. Finally, Section VIII concludes this article.

II. HYBRID TIME-VARYING WALKING DYNAMICS

This section introduces the modeling of the hybrid, time-varying dynamics of a quadrupedal robot that walks on a dynamic rigid platform. The model serves as a basis of the proposed controller design.
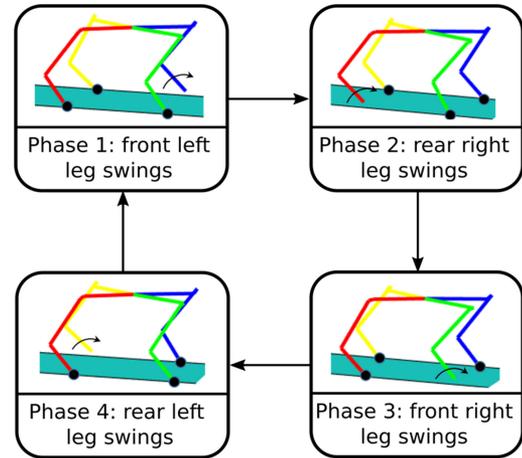

Fig. 1. Illustration of a complete quadrupedal walking cycle. Swing and stance legs are marked with arrows and circles, respectively.

Quadrupedal robot walking naturally involves hybrid dynamic behaviors. A complete quadrupedal walking cycle can be decomposed into four continuous phases connected by four discrete events, as illustrated in Fig. 1. When the swing leg moves in the air, the robot dynamics are continuous. When the swing leg strikes the walking surface, a foot-landing impact occurs and causes a sudden jump in the robot's joint velocities [7], which is sometimes referred to as a state-triggered jump.

Let $\mathbf{q}$ be the generalized coordinates of the robot, which is defined as

$$\mathbf{q} := \left[\mathbf{p}_b^T, \boldsymbol{\gamma}_b^T, q_1, q_2, \ldots, q_n \right]^T \in \mathcal{Q} \qquad (1)$$

where $\mathbf{p}_b := [x_b, y_b, z_b]^T$ is the vector of a robot's floating-base position with respect to the world coordinate frame, $\boldsymbol{\gamma}_b := [\phi_b, \theta_b, \psi_b]^T$ is the vector of the floating-base roll, pitch, and yaw angles with respect to the world coordinate frame, $[q_1 \, q_2 \ldots q_n]^T$ is the vector of the robot's joint angles, and $\mathcal{Q} \subset \mathbb{R}^{n+6}$ is the configuration space of the robot.

Let $\mathbf{u} \in U \subset \mathbb{R}^m$ be a vector of the robot's joint torques, where U is the set of admissible joint torques.

The degree of underactuation (DOU) of a walking quadrupedal robot can be computed as [20]

$$\text{DOU} = n + 6 - (n_{ct} - n_{ci}) - m \qquad (2)$$

where n_{ct} is the number of all holonomic constraints and n_{ci} is the number of internal constraints.

During three-dimensional (3-D) quadrupedal walking, $n_{ct} = 9$ and $n_{ci} = 3$. Suppose that all of the robot's joints are independently actuated. Then, DOU $= 0$. Thus, the robot is fully actuated, and all of its degrees of freedom (DOFs) can be directly commanded. The DOF can be calculated as

$$\text{DOF} = n + 6 - n_{ct}. \qquad (3)$$

The class of dynamic platforms considered in this article are dynamic platforms with a rigid surface, such as vessels, airplanes, and ground vehicles. As platform dynamics may be unknown or difficult to estimate during real-world robot operations, the

motion of a platform instead of its dynamics is considered in the derivation of the robot's dynamic model.

Modeling of the robot dynamics during a continuous phase and under a foot-landing impact is introduced next along with a mathematical definition of the impact event.

A. Continuous-Phase Dynamics

During a continuous phase of quadrupedal robot walking, three of the four legs contact the platform surface at their far ends (i.e., stance feet). Let $\mathbf{p}_c(\mathbf{q}) \in \mathbb{R}^{n_{ct}}$ be the position vector of the three stance feet in the world coordinate frame. When the stance feet do not slip on the platform surface, the associated holonomic constraints can be expressed as

$$\mathbf{J}_c\ddot{\mathbf{q}} + \dot{\mathbf{J}}_c\dot{\mathbf{q}} = \mathbf{A}_p(t) \tag{4}$$

where $\mathbf{J}_c(\mathbf{q}) := \frac{\partial \mathbf{p}_c}{\partial \mathbf{q}}(\mathbf{q})$. Note that the expressions of $\mathbf{J}_c$ during different continuous phases within a complete walking cycle are different because the stance feet are different. The variable $\mathbf{A}_p \in \mathbb{R}^{n_{ct}}$ is the vector of the platform accelerations at the contact points, which is explicitly time-dependent when the platform is dynamic.

With Lagrange's method, the continuous-phase dynamics of a quadrupedal robot that walks on a dynamic platform can be obtained as

$$\mathbf{M}(\mathbf{q})\ddot{\mathbf{q}} + \mathbf{C}(\mathbf{q}, \dot{\mathbf{q}}) := \mathbf{B}\mathbf{u} + \mathbf{J}_c^T \mathbf{F}_c \tag{5}$$

where $\mathbf{M}(\mathbf{q}) : \mathcal{Q} \to \mathbb{R}^{(n+6)\times(n+6)}$ is the inertia matrix, $\mathbf{C}(\mathbf{q}, \dot{\mathbf{q}}) : \mathcal{TQ} \to \mathbb{R}^{(n+6)\times 1}$ represents the sum of Coriolis, centrifugal, and gravitational terms, $\mathbf{B} \in \mathbb{R}^{(n+6)\times m}$ is the actuator selection matrix, and $\mathbf{F}_c \in \mathbb{R}^{n_{ct}}$ is the generalized external force induced by the contact between the robot's stance feet and the platform surface. Here, $\mathcal{TQ}$ is the tangent space of $\mathcal{Q}$.

From (4) and (5), $\mathbf{F}_c$ can be obtained as

$$\mathbf{F}_c = -(\mathbf{J}_c\mathbf{M}^{-1}\mathbf{J}_c^T)^{-1}(\mathbf{J}_c\mathbf{M}^{-1}(\mathbf{B}\mathbf{u} - \mathbf{C}) + \dot{\mathbf{J}}_c\dot{\mathbf{q}} - \mathbf{A}_p(t)). \tag{6}$$

Substituting (6) into (5) yields

$$\mathbf{M}(\mathbf{q})\ddot{\mathbf{q}} + \bar{\mathbf{C}}(t, \mathbf{q}, \dot{\mathbf{q}}) = \bar{\mathbf{B}}(\mathbf{q})\mathbf{u} \tag{7}$$

where $\bar{\mathbf{C}} := \mathbf{C} - \mathbf{J}_c^T(\mathbf{J}_c\mathbf{M}^{-1}\mathbf{J}_c^T)^{-1}(\mathbf{J}_c\mathbf{M}^{-1}\mathbf{C} - \dot{\mathbf{J}}_c\dot{\mathbf{q}} + \mathbf{A}_p(t))$ and $\bar{\mathbf{B}} := \mathbf{B} - \mathbf{J}_c^T(\mathbf{J}_c\mathbf{M}^{-1}\mathbf{J}_c^T)^{-1}(\mathbf{J}_c\mathbf{M}^{-1}\mathbf{B})$. Note that $\bar{\mathbf{C}}$ is explicitly time-dependent during dynamic-platform walking because $\mathbf{A}_p$ is explicitly time-dependent.

B. Switching Surface

When a swing foot strikes the platform surface, an impact occurs causing sudden jumps in the generalized velocities $\dot{\mathbf{q}}$. Thus, the foot-landing event connects a discrete impact and a continuous phase, which can be mathematically defined as the following switching surface S_q:

$$S_q(t, \mathbf{q}, \dot{\mathbf{q}}) := \{(t, \mathbf{q}, \dot{\mathbf{q}}) \in \mathbb{R}^+ \times \mathcal{TQ} : d_{\text{sw}}(t, \mathbf{q}) = 0$$

$$\dot{d}_{\text{sw}}(t, \mathbf{q}, \dot{\mathbf{q}}) < 0\} \tag{8}$$

where $d_{\text{sw}} : \mathbb{R}^+ \times \mathcal{Q} \to \mathbb{R}$ can be chosen as the shortest distance between the swing foot and the platform surface.

C. Discrete Impact Dynamics

Upon a swing-foot landing event, an impact occurs between the foot and the platform surface. Due to the instantaneous nature of the impact, the value of $\mathbf{q}$ remains continuous under an impact. However, the value of $\dot{\mathbf{q}}$ jumps.

Under an impulsive impact, the continuous dynamics in (5) and the holonomic constraint in (4) become

$$\mathbf{M}(\dot{\mathbf{q}}^+ - \dot{\mathbf{q}}^-) = \mathbf{J}_c^T \delta\mathbf{F}_c \text{ and } \mathbf{J}_c\dot{\mathbf{q}}^+ = \mathbf{V}_p^+ \tag{9}$$

where $\star^-$ and $\star^+$ represent the values of $\star$ right before and after the impact, respectively, $\delta\mathbf{F}_c$ is the impulsive impact force, and $\mathbf{V}_p$ is the vector of the platform velocities at the three contact points. The value of $\mathbf{V}_p$ also jumps because the platform velocities at the new foot-contact points right after the impact are not necessarily the same as the platform velocities at the previous foot-contact points right before the impact.

Rearranging the abovementioned equation gives

$$\begin{bmatrix} \dot{\mathbf{q}}^+ \\ \delta\mathbf{F}_c \end{bmatrix} = \begin{bmatrix} \mathbf{M}(\mathbf{q}) & -\mathbf{J}_c^T(\mathbf{q}) \\ \mathbf{J}_c^T(\mathbf{q}) & \mathbf{0}_{n_{ct}\times n_{ct}} \end{bmatrix}^{-1} \begin{bmatrix} \mathbf{M}(\mathbf{q})\dot{\mathbf{q}}^- \\ \mathbf{V}_p^+ \end{bmatrix} \tag{10}$$

where $\mathbf{0}_{n_{ct}\times n_{ct}}$ is a $n_{ct} \times n_{ct}$ zero matrix. Equation (10) can, then, be used to obtain the jump in the generalized velocities as

$$\dot{\mathbf{q}}^+ := \mathbf{R}(t, \mathbf{q})\dot{\mathbf{q}}^- \tag{11}$$

where $\mathbf{R} : \mathbb{R}^+ \times Q \to \mathbb{R}^{(n+6)\times(n+6)}$. Note that the expression of $\mathbf{R}$ is explicitly time-dependent because $\mathbf{R}$ contains the explicitly time-dependent function $\mathbf{V}_p$. Also, the expressions of $\mathbf{R}$ during different continuous phases within a complete walking cycle are different because the expressions of the corresponding Jacobian matrices $\mathbf{J}_c$ are different.

The model derived in this section clearly shows that the dynamics of a robot that walks on a dynamic platform are hybrid, time-varying, and involve state-triggered jumps that cannot be directly controlled due to their infinitesimally short periods of duration.

III. MODEL-BASED FEEDBACK CONTROL DURING CONTINUOUS PHASES

This section introduces a continuous-phase control law that provably stabilizes continuous-phase quadrupedal walking over dynamic rigid platforms. To guarantee that the control law also provably stabilizes the overall hybrid walking process, a Lyapunov-based stability analysis is performed as explained in Section IV.

A. Continuous Model-Based Control

In this article, stable walking over dynamic platforms is achieved through the provable stabilization of the hybrid, time-varying control system.

Let $\mathbf{h}(\mathbf{q})$ and $\mathbf{h}_d(t, \mathbf{q})$ be the control variables and their reference trajectories, respectively. Suppose that all of the robot's joints are independently actuated, i.e., $m = n$, and that $\mathbf{h}_d(t, \mathbf{q})$ is smooth in t within each continuous domain. Then, by (2), the robot is fully actuated. Thus, the number of control variables can
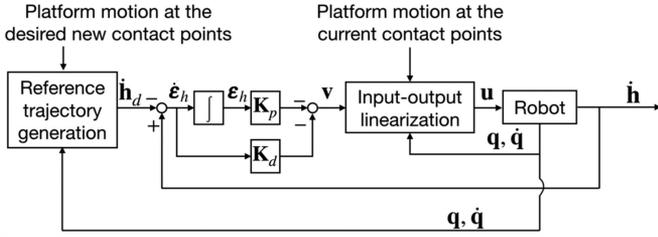
Fig. 2. Block diagram of the proposed continuous-phase control law.

be chosen as the same as the robot's DOF. From (3), we have $\mathbf{h} \in \mathbb{R}^{n+6-n_{ct}}$.

The trajectory tracking error can be defined as

$$\boldsymbol{\epsilon}_h(t, \mathbf{q}) := \mathbf{h}(\mathbf{q}) - \mathbf{h}_d(t, \mathbf{q}). \tag{12}$$

The control objective is then: to drive $\|\boldsymbol{\epsilon}_h\|$ to a bounded small number at the steady state for the overall hybrid closed-loop system.

Since the discrete impact dynamics cannot be directly controlled due to their infinitesimally short periods of duration, we choose to derive a continuous control law to directly stabilize the continuous-phase dynamics.

The proposed continuous control law is derived based on the full-order model of the continuous-phase walking dynamics, as derived in Section II-A. A block diagram of the proposed control law is shown in Fig. 2.

To simplify the controller design, input–output linearization [21] is utilized to transform the continuous-phase nonlinear dynamics into a linear system.

With the trajectory tracking error $\boldsymbol{\epsilon}_h$ chosen as the output function $\mathbf{y}$, we have $\dot{\mathbf{y}} = \frac{\partial \boldsymbol{\epsilon}_h}{\partial \mathbf{q}} \dot{\mathbf{q}} + \frac{\partial \boldsymbol{\epsilon}_h}{\partial t}$ and $\ddot{\mathbf{y}} = \frac{\partial}{\partial \mathbf{q}}\left(\frac{\partial \boldsymbol{\epsilon}_h}{\partial \mathbf{q}} \dot{\mathbf{q}}\right) \dot{\mathbf{q}} + \frac{\partial \boldsymbol{\epsilon}_h}{\partial \mathbf{q}} \ddot{\mathbf{q}} + \frac{\partial^2 \boldsymbol{\epsilon}_h}{\partial t^2}$. From (7), we have $\ddot{\mathbf{q}} = \mathbf{M}^{-1}(\bar{\mathbf{B}}\mathbf{u} - \bar{\mathbf{C}})$. Substituting the expression of $\ddot{\mathbf{q}}$ into the expression of $\ddot{\mathbf{y}}$, we have $\ddot{\mathbf{y}} = \frac{\partial}{\partial \mathbf{q}}\left(\frac{\partial \boldsymbol{\epsilon}_h}{\partial \mathbf{q}} \dot{\mathbf{q}}\right) \dot{\mathbf{q}} + \frac{\partial \boldsymbol{\epsilon}_h}{\partial \mathbf{q}} \mathbf{M}^{-1}(\bar{\mathbf{B}}\mathbf{u} - \bar{\mathbf{C}}) + \frac{\partial^2 \boldsymbol{\epsilon}_h}{\partial t^2}$.

Thus, by choosing a continuous control law as

$$\mathbf{u} = \left(\frac{\partial \boldsymbol{\epsilon}_h}{\partial \mathbf{q}} \mathbf{M}^{-1} \bar{\mathbf{B}}\right)^* \left(\frac{\partial \boldsymbol{\epsilon}_h}{\partial \mathbf{q}} \mathbf{M}^{-1} \bar{\mathbf{C}} - \frac{\partial}{\partial \mathbf{q}}\left(\frac{\partial \boldsymbol{\epsilon}_h}{\partial \mathbf{q}} \dot{\mathbf{q}}\right) \dot{\mathbf{q}} - \frac{\partial^2 \boldsymbol{\epsilon}_h}{\partial t^2} + \mathbf{v}\right) \tag{13}$$

where $(\cdot)^*$ denotes the pseudoinverse of a matrix $(\cdot)$, we obtain the linearized output function dynamics as $\ddot{\mathbf{y}} = \mathbf{v}$.

Define $\mathbf{v}$ as a proportional-derivative (PD) control law

$$\mathbf{v} = -\mathbf{K}_p \mathbf{y} - \mathbf{K}_d \dot{\mathbf{y}} \tag{14}$$

where $\mathbf{K}_p$ and $\mathbf{K}_d$ are PD gains. Then, the closed-loop dynamics during continuous phases are $\ddot{\mathbf{y}} = -\mathbf{K}_p \mathbf{y} - \mathbf{K}_d \dot{\mathbf{y}}$.

By properly assigning values for the PD gains, the proposed input–output linearizing control law can provably guarantee the stability of the closed-loop control system during continuous phases.

However, due to the presence of the uncontrolled impact dynamics, the proposed control law cannot automatically guarantee the provable stabilization of the overall hybrid, time-varying walking dynamics. To derive sufficient conditions under which the proposed control law can provably solve the stabilization

problem, the stability of the closed-loop system is analyzed in Section IV.

Before introducing the stability analysis, we first introduce the construction of impact invariance that can be used to satisfy a necessary condition for asymptotic stabilization.

B. Impact Invariance Construction

If $\mathbf{y}^+ = \mathbf{0}$ and $\dot{\mathbf{y}}^+ = \mathbf{0}$ hold when $\mathbf{y}^- = \mathbf{0}$ and $\dot{\mathbf{y}}^- = \mathbf{0}$ under an impact, then $\mathbf{y}$ and $\dot{\mathbf{y}}$ are called "impact invariant" [7]. The impact invariance condition essentially requires that the reference trajectory should respect the impact dynamics. It is a necessary condition for achieving asymptotic stabilization of hybrid systems with state-triggered jumps that include the robot dynamics, as derived in Section II.

To meet the impact invariance condition, we have previously derived a method of constructing impact invariance [19] for the design of trajectory tracking controllers for legged locomotion on static platforms. The method translates the condition into equality constraints and enforces the constraints through trajectory generation. In this article, we extend the previous method from the controller design for legged locomotion on static platforms to dynamic platforms.

Consider a complete gait cycle of quadrupedal robot walking. Let $\mathbf{q} = \mathbf{q}_d(t) \in \mathbb{R}^{n+6}$ be the solution to the equation $\mathbf{h}(\mathbf{q}) - \mathbf{h}_d(t, \mathbf{q}) = \mathbf{0}$. By definition, to meet the impact invariance condition, the following equations should hold:

$$\mathbf{q}_d(\tau_{k,i}^+) = \mathbf{q}_d(\tau_{k,i}^-); \quad \mathbf{q}_d(\tau_{k,0}^+) = \mathbf{q}_d(\tau_{k,4}^-) \tag{15}$$

$$\dot{\mathbf{q}}_d(\tau_{k,i}^+) = \mathbf{R}(\tau_{k,i}, \mathbf{q}_d(\tau_{k,i}^-))\dot{\mathbf{q}}_d(\tau_{k,i}^-)$$

$$\dot{\mathbf{q}}_d(\tau_{k,0}^+) = \mathbf{R}(\tau_{k,4}, \mathbf{q}_d(\tau_{k,4}^-))\dot{\mathbf{q}}_d(\tau_{k,4}^-). \tag{16}$$

Here, $i \in \{1, 2, 3\}$, and $0 < \tau_{k,0} < \tau_{k,1} < \tau_{k,2} < \tau_{k,3} < \tau_{k,4}$. The variables $\tau_{k,0}^+$ and $\tau_{k,4}^-$ are the initial and the final instants of the complete kth gait cycle ($k \in \{1, 2, 3, \ldots\}$). The variable $\tau_{k,i}$ ($i \in \{1, 2, 3\}$) is the planned instant of a foot-landing event between $t = \tau_{k,0}^+$ and $t = \tau_{k,4}^-$.

Equation (15) always holds due to the continuity of the generalized coordinates $\mathbf{q}$ under an impact. Thus, to construct impact invariance, only (16) needs to be enforced through trajectory generation as explained in Section V.

IV. CLOSED-LOOP STABILITY ANALYSIS

This section presents the stability analysis of the closed-loop hybrid, time-varying system under the proposed continuous control law. The analysis result is a set of sufficient conditions that the proposed controller should satisfy in order to provably stabilize the hybrid closed-loop control system for achieving stable walking on dynamic rigid platforms.

Define $\mathbf{x} := [\mathbf{y}^T \ \dot{\mathbf{y}}^T]^T$. Under the proposed continuous-phase control law in (13) and (14), the closed-loop output function dynamics can be compactly expressed as

$$\begin{cases} \dot{\mathbf{x}} = \mathbf{A}\mathbf{x}, & \text{if } (t, \mathbf{x}^-) \notin S(t, \mathbf{x}) \\ \mathbf{x}^+ = \boldsymbol{\Delta}(t, \mathbf{x}^-), & \text{if } (t, \mathbf{x}^-) \in S(t, \mathbf{x}) \end{cases} \tag{17}$$

where $\mathbf{A} := \begin{bmatrix} \mathbf{0} & \mathbf{I} \\ -\mathbf{K}_p & -\mathbf{K}_d \end{bmatrix}$, $\mathbf{0}$ and $\mathbf{I}$ are zero and identity matrices with appropriate dimensions, and the expressions of S and $\boldsymbol{\Delta}$ can be obtained from the switching surface S_q in (8), the reset map $\mathbf{R}$ in (11), and the trajectory tracking error ϵ_h in (12). For notational simplicity, one continuous phase and the subsequent discrete jump of a complete walking cycle are given in (17).

The continuous-phase dynamics can be provably stabilized by properly selecting the PD gains such that $\mathbf{A}$ is Hurwitz. However, the instantaneous, uncontrolled impact dynamics cannot be directly regulated. Hence, we will utilize the construction of multiple Lyapunov functions [22] to derive sufficient conditions for the overall hybrid, time-varying closed-loop system.

The proposed stability analysis is an extension of our previous work on trajectory tracking control of static-platform locomotion [19]. The previous analysis cannot be directly performed on the hybrid, time-varying system in (17) because it does not consider the time dependence of the system dynamics induced by the platform motion. To this end, this article extends the previous analysis with the consideration of platform motions as summarized in the following assumption.

A1) The platform acceleration at the foot-contact points $\mathbf{A}_p(t)$ is differentiable in t within a continuous phase.

The assumption (A1) is valid for real-world dynamic rigid platforms such as vessels moving in regular waves [23].

Before explaining the proposed stability analysis, several related variables and concepts are first introduced.

Let τ_k and t_k be the planned and the actual kth impact timings, respectively. The variables t_k^- and t_k^+ denote the time instants right before and after the kth impact, respectively. For notational simplicity, $\star(t_{k-1}^-)$ and $\star(t_{k-1}^+)$ are denoted as $\star|_{k-1}^-$ and $\star|_{k-1}^+$, respectively, for the rest of this article.

A fictitious system is introduced and defined as $\dot{\bar{\mathbf{x}}} := \mathbf{A}\bar{\mathbf{x}}$ such that under the initial condition $\bar{\mathbf{x}}(t_0) = \mathbf{x}_0$, a solution of the system is given by $\bar{\mathbf{x}}(t; t_0, \mathbf{x}_0) \forall t > t_0$. Then, the solution to the actual continuous-phase system between the $(k-1)$th and the kth impacts satisfies

$$\mathbf{x}(t) = \bar{\mathbf{x}}(t; t_{k-1}^+, \mathbf{x}|_{k-1}^+) \quad \forall t \in (t_{k-1}, t_k]. \tag{18}$$

Theorem (Closed-loop stability conditions): The closed-loop control system in (17) is locally asymptotically stable if the following two conditions are met.

C1) Reference trajectories are planned with the impact invariance condition met to respect the impact dynamics.

C2) The PD gains are chosen such that $\mathbf{A}$ is Hurwitz and that the state $\mathbf{x}$ converges to zero sufficiently fast during continuous phases. ∎

Proof: By the theory of multiple Lyapunov functions [22], a hybrid system is asymptotically stable if there exists a Lyapunov function candidate and a positive number r such that for all $\mathbf{x}|_0^+ \in B_r(\mathbf{0}) := \{\mathbf{x} : \|\mathbf{x}\| \leq r\}$, the following two conditions hold: 1) the Lyapunov function candidate asymptotically decreases during each continuous phase and 2) its values at the initial instants of all continuous phases form a strictly decreasing sequence.

We begin the stability analysis with continuous phases.

Suppose that the PD gains are chosen such that the matrix $\mathbf{A}$ is Hurwitz. Then, there exists a Lyapunov function candidate $V(\mathbf{x})$ and positive numbers c_1, c_2, and c_3 such that

$$c_1\|\mathbf{x}\|^2 \leq V(\mathbf{x}) \leq c_2\|\mathbf{x}\|^2 \text{ and } \dot{V}(\mathbf{x}) \leq -c_3\|\mathbf{x}\|^2 \tag{19}$$

hold for all $\mathbf{x}$ during continuous phases [21]. Then,

$$V|_k^+ \leq e^{-\frac{c_3}{c_2}(t_k - t_{k-1})} V|_{k-1}^+, \ k \in \{1, 2, \ldots\}. \tag{20}$$

Next, the evolution of the Lyapunov function candidate V across a state-triggered jump is analyzed. By the triangle inequality principle, the norm of the state $\mathbf{x}$ right after the kth impact can be approximated as

$$\|\mathbf{x}|_k^+\| = \|\boldsymbol{\Delta}(t_k, \mathbf{x}|_k^-)\| \leq \|\boldsymbol{\Delta}(t_k, \mathbf{x}|_k^-) - \boldsymbol{\Delta}(\tau_k, \mathbf{x}|_k^-)\|$$
$$+ \|\boldsymbol{\Delta}(\tau_k, \mathbf{x}|_k^-) - \boldsymbol{\Delta}(\tau_k, \mathbf{0})\| + \|\boldsymbol{\Delta}(\tau_k, \mathbf{0})\|. \tag{21}$$

By the condition (C1), we have $\boldsymbol{\Delta}(\tau_k, \mathbf{0}) = \mathbf{0}$.

Under the assumption (A1), the platform velocity at the foot-contact points $\mathbf{V}_p(t)$ is continuously differentiable in t. Then, (11) and the definition of $\mathbf{x}$ indicate that $\boldsymbol{\Delta}(t, \mathbf{x})$ is locally continuously differentiable in t and $\mathbf{x}$. Thus, there exist Lipschitz constants L_{Δ_t} and L_{Δ_x} and a positive number r_Δ such that for any $\mathbf{x}|_0^+ \in B_{r_\Delta}(\mathbf{0})$, we have

$$\|\Delta(t_k, \mathbf{x}|_k^-) - \Delta(\tau_k, \mathbf{x}|_k^-)\| \leq L_{\Delta_t}\|t_k - \tau_k\| \tag{22}$$
$$\|\Delta(\tau_k, \mathbf{x}|_k^-) - \Delta(\tau_k, \mathbf{0})\| \leq L_{\Delta_x}\|\mathbf{x}|_k^-\|. \tag{23}$$

Since the continuous-phase dynamics of the hybrid system in (17) is defined by a function (i.e., $\mathbf{Ax}$) that is continuously differentiable in $\mathbf{x}$, there exists a Lipschitz constant L_t and a positive number r_t such that the difference between the actual and the planned kth impact timings can be approximated as [24]

$$\|t_k - \tau_k\| \leq L_t\|\bar{\mathbf{x}}(\tau_k; t_{k-1}^+, \mathbf{x}|_{k-1}^+)\| \tag{24}$$

for all $\mathbf{x}|_0^+ \in B_{r_t}(\mathbf{0})$.

Combining (22) and (24) yields

$$\|\boldsymbol{\Delta}(t_k, \mathbf{x}|_k^-) - \boldsymbol{\Delta}(\tau_k, \mathbf{x}|_k^-)\| \leq L_{\Delta_t} L_t \|\bar{\mathbf{x}}(\tau_k; t_{k-1}^+, \mathbf{x}|_{k-1}^+)\|. \tag{25}$$

From (21)–(25), we have

$$\|\mathbf{x}_k^+\| \leq L_{\Delta_t} L_t \|\bar{\mathbf{x}}(\tau_k; t_{k-1}^+, x_{k-1}^+)\| + L_{\Delta_x}\|\mathbf{x}_k^-\| \tag{26}$$

for any $\mathbf{x}_0^+ \in B_r(0)$, where $r := \min(r_\Delta, r_t)$.

From (19) and (20), we have

$$\|\mathbf{x}|_k^-\| \leq \sqrt{\frac{c_2}{c_1}} e^{-\frac{c_3}{2c_2}(t_k - t_{k-1})} \|\mathbf{x}|_{k-1}^+\| \tag{27}$$

$$\|\tilde{\mathbf{x}}|_k^-\| \leq \sqrt{\frac{c_2}{c_1}} e^{-\frac{c_3}{2c_2}(\tau_k - t_{k-1})} \|\mathbf{x}|_{k-1}^+\|. \tag{28}$$

From (26)–(28), we have $\|\mathbf{x}|_k^+\| \leq \sqrt{\frac{c_2}{c_1}}(L_{\Delta_t} L_t + L_{\Delta_x} e^{-\frac{c_3}{2c_2}(t_k - \tau_k)})e^{-\frac{c_3}{2c_2}(\tau_k - t_{k-1})}\|\mathbf{x}|_{k-1}^+\|$.

By the condition (C2), the PD gains can be assigned to allow a sufficiently high convergence rate. Then, suppose that the PD gains are chosen such that $e^{-\frac{c_3}{2c_2}(t_k - \tau_k)} \leq 1 + \epsilon$ holds for some positive number ϵ. Then, for any $\mathbf{x}|_0^+ \in B_r(\mathbf{0})$, we have $\|\mathbf{x}|_k^+\| \leq$

$\sigma \|\mathbf{x}\|_{k-1}^{+}\|$ with

$$\sigma := \sqrt{\tfrac{c_2}{c_1}}(L_{\Delta_t}L_t + L_{\Delta_x}(1+\epsilon))e^{-\tfrac{c_3}{2c_2}\Delta\tau_k}$$

and $\Delta\tau_k := \tau_k - t_{k-1}$. Therefore, $V|_k^+ \le \Omega V|_{k-1}^+$, $\Omega := \frac{c_2\sigma^2}{c_1}$.

If the PD gains are chosen such that $\mathbf{A}$ is Hurwitz and that $\frac{c_2\sigma^2}{c_1} < 1$ holds (i.e., $\Omega < 1$), then $V|_0^+$, $V|_1^+$, $V|_2^+ \ldots$ form a strictly decreasing sequence. By the definition of σ, if the continuous-phase convergence rate $\frac{c_3}{c_2}$ can be chosen sufficiently large, then $\sigma < \sqrt{\frac{c_1}{c_2}}$ holds (i.e., $\frac{c_2\sigma^2}{c_1} < 1$ is satisfied). Then, by the stability theory based on the construction of multiple Lyapunov functions, the closed-loop hybrid system is locally asymptotically stable for any $\mathbf{x}|_0^+ \in B_r(\mathbf{0})$. ∎

V. REFERENCE TRAJECTORY GENERATION

This section explains the proposed trajectory generation method for planning the desired quadrupedal walking motions on dynamic rigid platforms.

A. Formulation of a Model-Based Optimization Problem

In this article, the problem of trajectory generation is formulated as an optimization problem. The solution of the optimization problem is the reference trajectories $\mathbf{h}_d$, which represent kinematically and dynamically feasible walking motions over dynamic rigid platforms.

The formulation of the optimization problem begins with properly defining $\mathbf{h}_d$. Without loss of generality, $\mathbf{h}_d$ is defined based on walking pattern encoding [7]. A walking pattern represents the relative evolution of configuration-based variables with respect to a phase variable that presents how far or how long a robot has walked within a gait cycle. Let θ be the phase variable. Let θ^+ and θ^- be the planned values of θ at the beginning and the end of a complete gait cycle, respectively. Then, the normalized phase variable s is defined as $s(\theta) := \frac{\theta-\theta^+}{\theta^--\theta^+}$. The desired walking pattern of the control variable $\mathbf{h}$ can be encoded by $s(\theta)$ as $\mathbf{h}(\mathbf{q}) - \mathbf{h}_d(s(\theta)) = \mathbf{0}$. The Nth-order Bézier curves can be used to define $\mathbf{h}_d$ as $\mathbf{h}_d(s) := \sum_{i=0}^{N} \boldsymbol{\alpha}_i \frac{N!}{i!(N-i)!}s^i(1-s)^{N-i}$. Here, $\boldsymbol{\alpha}_i \in \mathbb{R}^{n+6-n_{ct}}$ are the coefficients of the Bézier curves, and are in turn used as optimization variables.

The cost function of the optimization problem can be chosen as the energy consumed during walking [7].

Necessary constraints are considered to ensure that the optimized reference trajectories would correspond to kinematically and dynamically feasible quadrupedal locomotion over dynamic rigid platforms. These constraints include the following:

1) switching surfaces as derived in Section II-B;
2) the impact invariance condition derived in Section III-B;
3) joint position and velocity limits;
4) joint torque limits with the torque from (13);
5) platform-contact constraints (e.g., unilateral constraints and friction-cone constraints) with the contact force from (6);
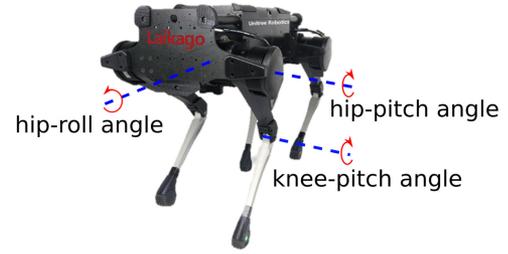6) desired gait features (e.g., the desired duration of gait cycle).

Fig. 3. Laikago quadrupedal robot (developed by Unitree) used for experimental validation. Each leg of the robot has three actuated joints, which are hip-roll, hip-pitch, and knee-pitch joints.

Both continuous-phase and discrete dynamics are contained in the constraints. The continuous-phase dynamics in (5) are contained in the joint torque limits and the platform-contact constraints. The discrete impact dynamics in (11) are contained in the impact invariance condition.

The platform motions (e.g., $\mathbf{V}_p$ and $\mathbf{A}_p$) are also contained in the constraints because the platform motion directly affects the contact force between the robot and the platform, the occurrence of a swing-foot landing event, and the impact dynamics, as explained in Section II.

B. Optimization Setup

The optimization is set up as a nonlinear programming (NLP) problem. The software tool used to solve the NLP is MATLAB's fmincon command. As the focus of this article is on controller design, the planning is solved offline.

The control variables $\mathbf{h}$ are chosen as the base pose (i.e., position and orientation) and swing-foot position, i.e., $\mathbf{h}(\mathbf{q}) := \left[\mathbf{p}_b^T(\mathbf{q}), \boldsymbol{\gamma}_b^T(\mathbf{q}), \mathbf{p}_{sw}^T(\mathbf{q})\right]^T$.

In general, the phase variable θ can be defined based on either generalized coordinates $\mathbf{q}$ [7] or time t [19].

In this article, θ is defined as time-dependent, i.e., $\theta(t) := t - \tau_k$, $k \in \{1, 2, \ldots\}$ during the kth walking cycle (i.e., $t \in (t_k, t_{k+1}]$). Thus, θ represents the current instant relative to the planned initial instant of the kth walking cycle. With the phase variable chosen as time-based, the reference trajectories $\mathbf{h}_d$ become functions of t alone, i.e., $\mathbf{h}_d(t, \mathbf{q}) = \mathbf{h}_d(t)$.

VI. SIMULATIONS AND EXPERIMENTS

This section presents the validation results obtained through simulations and experiments.

A. Simulation and Experimental Setup

In this article, MATLAB simulations are used to validate the theoretical control law derived in Section III. Simulations on PyBullet, which is a 3-D realistic robot simulator [25], are conducted to gain preliminary insight into the controller implementation on hardware. Experiments on a physical quadrupedal robot (see Fig. 3) are used to evaluate the effectiveness of the proposed control approach as well.

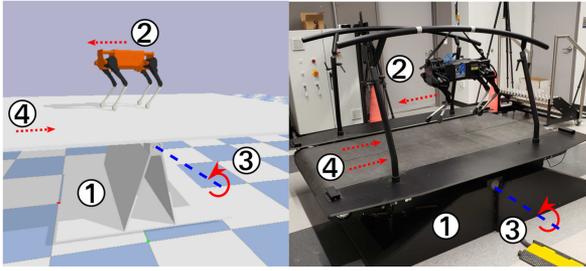The dynamic rigid platform used for validation is as follows.

Fig. 4. PyBullet simulation and experimental set-up for assessing the performance of the proposed control strategy. ①: Treadmill. ②: Laikago robot and its walking direction. ③: Rotating axis of the treadmill. ④: Moving direction of the treadmill belt.

Fig. 6. Trajectory tracking results with gait (G1). (a) Joint position trajectories. (b) Base roll and pitch trajectories. (c) Joint torque profiles of the rear-left leg.
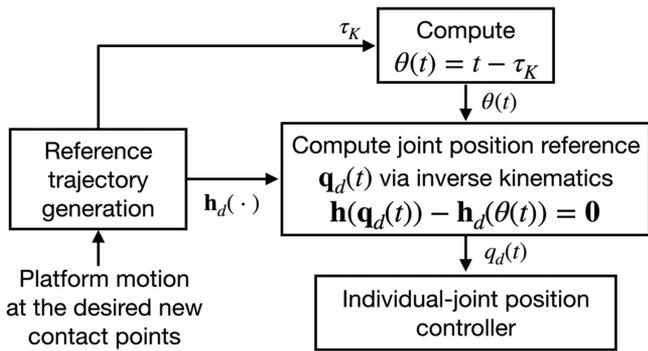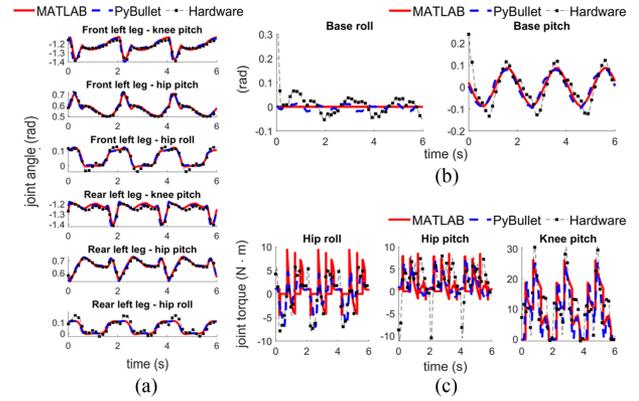

Fig. 5. Flow chart of the controller implementation procedure used in PyBullet simulations and hardware experiments.

P1) A platform with a whole-body pitching motion and a surface translating motion (Nominal pitching amplitude $= \pm 5°$. Nominal pitching frequency $= 0.5$ Hz).

In experiments, the platform (P1) is chosen as a pitching treadmill with translating belts on the surface.

To validate the proposed control approach during walking motions with different gait characteristics, three sets of reference trajectories are used in simulations and experiments. They are generated using the optimization-based planning method in Section V. The gait characteristics are as follows.

G1) Step length $= 10$ cm. Maximum swing-foot height $= 6$ cm. (Treadmill belt speed $= 5$ cm/s).

G2) Step length $= 16$ cm. Maximum swing-foot height $= 6$ cm. (Treadmill belt speed $= 8$ cm/s).

G3) Step length $= 16$ cm. Maximum swing-foot height $= 9$ cm. (Treadmill belt speed $= 8$ cm/s).

For simplicity, the optimization enforces the exact correspondence between the duration of the reference gait cycle and one period of the platform pitching motion. Due to the space limitation, these reference trajectories are displayed in Figs. 4–6 in the supplementary file.

As it is assumed that the platform motion is known (i.e., sensed or estimated) in the theoretical controller design, we added perturbations to the platform motion for assessing the robustness of the proposed control approach under uncertainties. Two sets of perturbations are implemented with the platform (P1), including the following.

U1) Uncertainties in the pitching amplitude.

U2) Uncertainties in the belt speed.

More details on the set-ups of MATLAB and PyBullet simulations as well as experiments are given as follows.

MATLAB Simulation Setup: The robot model derived in Section II is used to simulate the closed-loop system under the control law in (13) and (14). The PD gains for gait (G1) are chosen as $\mathbf{K}_p = \text{diag}(100, 36, 110, 100, 36, 110, 36, 64, 110)$ and $\mathbf{K}_d = \text{diag}(20, 12, 21, 20, 12, 21, 12, 16, 21)$, yielding closed-loop poles with negative real parts between -10.5 and -6. The PD gains for the uncertainty case (U1) are chosen the same as gait (G1). Due to the space limitation, the PD gains for other cases are included in the supplementary file.

PyBullet Simulation Setup: A 3-D realistic robot model that closely emulates the physical and geometric properties of the physical quadrupedal robot is used in the simulation, as shown in Fig. 4. The "PD" control gains are set as 1.0 and 0.25, respectively. Note that these values may not reflect the true PD gains implemented in PyBullet due to the intrinsic gain multipliers used in the simulator.

Experimental Setup: The experimental setup consists of a quadrupedal robot and a treadmill, as shown in Fig. 4. The "PD gains" of the joint-level controllers are set as 5.5 and 0.2, respectively. Similar to PyBullet, these values may not reflect the true PD gains implemented on the physical robot's joint motors due to the intrinsic gain multipliers of the hardware. These PD gains in MATLAB, PyBullet, and experiments are tuned to produce similar continuous-phase convergence rates.

The treadmill used in the experiment is a split-belt Motek M-gait treadmill [26], which is capable of performing preprogrammed sinusoidal pitching motions. Its dimension is: 2.3 m (length) by 1.82 m (width) by 0.5 m (height). Its total mass is 750 kg. Each of its two belts is powered by a 4.5 kW servo motor. During experiments, the motion of the two belts is always synchronized.

The physical robot used for experimental validation is a quadrupedal Laikago robot developed by Unitree [27] (see Fig. 3). Its dimension is 0.56 m (length) by 0.35 m (width) by 0.6 m (height). Its total mass is 25 kg, and each leg weighs

2.9 kg. Each leg has three independently actuated joints, i.e., hip-roll, hip-pitch, and knee-pitch joints, with a power density of 0.80 kW/kg and a torque limit of 20 Nm, 55 Nm, and 55 Nm, respectively. These torque limits are incorporated into the robot models used for the controller implementation in MATLAB and PyBullet simulations.

B. Controller Implementation in PyBullet and Experiments

In PyBullet simulations and experiments, the proposed control law in (13) and (14), which is a torque command, is implemented as an individual-joint PD controller, which is preferred in robot walking experiments in the presence of model uncertainties [7]. Accordingly, the original reference trajectories $\mathbf{h}_d$ are converted into joint-position reference trajectories $\mathbf{q}_d(t)$, which are then sent to the robot's individual-joint controllers, as illustrated in Fig. 5.

C. Validation Results With a Periodically Pitching Rigid Platform

Validation results obtained from MATLAB, PyBullet, and experiments with the reference gait (G1) and the platform (P1) are displayed in Fig. 6. The joint trajectory tracking results in Fig. 6(a) demonstrates the reliable tracking performance of the proposed control approach across simulations and experiments. The base roll and pitch trajectories in Fig. 6(b) show that the robot maintains a relatively steady base pose, indicating stable walking on the pitching platform.

Joint torque profiles in Fig. 6(c) overall show relatively consistent trends between simulations and experiments. Note that the hip-pitch torque profile obtained through experiments shows peaks of -10 Nm near 2 s and 4 s, whereas MATLAB and PyBullet results do not exhibit such jumps near those time instants. This might be caused by the impact modeling discrepancies between the physical robot and the simulated robots. During the experiment, the rear-left leg of the physical robot slightly rebounds near those time instants right after the rear-right leg strikes the platform surface. However, such rebounding behavior is not captured by the dynamic model, as derived in Section II.

The validation results obtained with the gaits (G2) and (G3) demonstrate similar effectiveness of the proposed control approach. Due to the space limitation, these results are displayed in Figs. 1 and 2 in the supplementary file.

D. Validation Results on Robustness

To assess the robustness of the proposed control approach under uncertainties such as sensor noise and estimation errors, perturbations in the platform motions are implemented in both simulations and experiments.

With the uncertainties (U1), up to $\pm 20\%$ uncertainties, which approximately correspond to a variation of 4 cm in the stance-foot height, are added to the nominal pitching amplitude of the platform. Fig. 7 displays the walking control results obtained from MATLAB, PyBullet, and experiments with the reference gait (G1) and under the uncertainties (U1). The results match
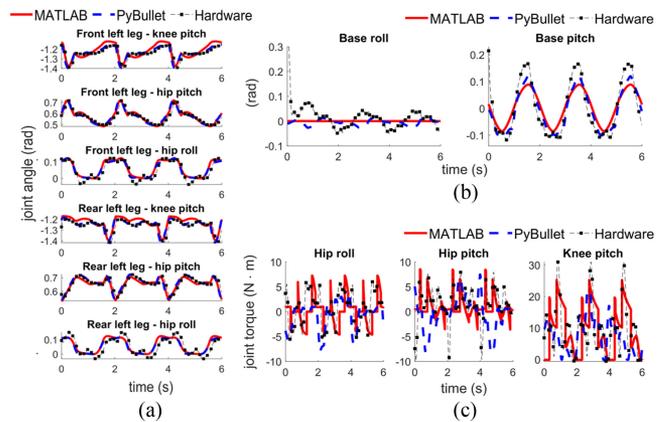

Fig. 7. Trajectory tracking results with gait (G1) under uncertainties (U1). (a) Joint position trajectories. (b) Base roll and pitch trajectories. (c) Joint torque profiles of the rear-left leg.

relatively closely with those obtained without the uncertainties (U1) in Fig. 6, which demonstrates the robustness of the proposed controller in mitigating a relatively moderate level of uncertainties.

With the uncertainties (U2), up to $\pm 20\%$ uncertainties, which approximately correspond to a variation of 8 cm in the stance-foot height over 10 gait cycles, are added to the belt speed of the treadmill. The robot's motion was shaky during experiments, but the robot was able to sustain motion for over twenty steps, which indicates that the inherent robustness of the proposed control approach is able to tackle the implemented uncertainties in the treadmill belt speed. Due to the space limitation, these results are displayed in Fig. 3 in the supplementary file.

E. Comparative Simulations of a Static-Platform Controller

A controller designed for static-platform locomotion is simulated to demonstrate the necessity of explicitly accounting for the time-varying robot dynamics induced by platform movement through controller design. The controller is chosen as our previous control approach for static-platform locomotion [19], which does not account for the time-varying robot dynamics induced by platform movement. The "PD" gains for PyBullet simulations are set as 1.0 and 0.25, respectively.

Fig. 8(a) shows the robot's base pose trajectories during static-terrain walking in PyBullet, which indicates a relatively steady base pose and, thus, demonstrates stable walking motions on the static terrain. However, the controller fails to sustain stable walking when the robot walks on a pitching platform (i.e., the platform (P1)], as revealed by the irregular base motion in the two trials in Fig. 8(b).

VII. DISCUSSION

This article has derived a model-based control approach that achieves stable quadrupedal locomotion over dynamic rigid platforms by explicitly addressing the associated hybrid, time-varying robot dynamics. Thanks to the inherent robustness of
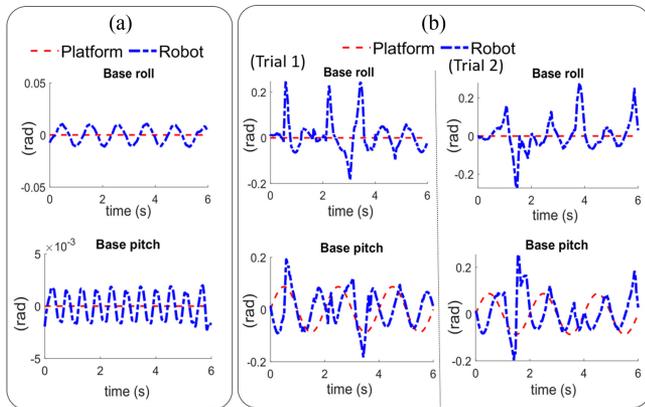
Fig. 8. Comparative simulation results of the robot's base pose trajectories under a controller designed for static platforms, obtained during. (a) Walking on a static platform. (b) Walking on the dynamic platform (P1).

feedback control, the controller demonstrates robustness under moderate levels of platform motion uncertainties, which indicates that the proposed control could be effective even in the presence of uncertainties caused by platform motion estimation. Despite the impressive estimation accuracy achieved by recent studies on static-platform legged locomotion [28], [29], state estimation for dynamic-platform locomotion remains an open question. To this end, we will investigate state estimator design for dynamic-platform locomotion and integrate the estimator with the proposed control approach in our future work.

To enhance the robustness of the proposed control approach for real-world robot applications, we will extend the construction of multiple Lyapunov functions to synthesize robust control laws for hybrid, time-varying systems that include quadrupedal robots traversing dynamic rigid platforms. Uncertainties that we plan to address include model discrepancies, state estimation errors, and disturbances.

To enable robot locomotion over dynamic platforms with complex, nonperiodic motions, online motion planning techniques will be demanded in addition to a reliable control approach. Online motion planning for legged robots is a challenging problem because of the associated high computational burden. To reduce the computation burden, we will explore the possibility of using a reduced-order robot model instead of a full-order one in online motion planning. This approach is potentially promising because a physical quadrupedal robot typically has a heavy trunk and lightweight legs and, thus, may be relatively accurately described by a reduced-order model.

VIII. CONCLUSION

In this article, we have introduced a control approach that realizes stable quadrupedal robot locomotion on dynamic rigid platforms by provably stabilizing the associated hybrid, time-varying control system. The model of a quadrupedal robot that walks on a dynamic rigid platform was formulated as a hybrid, time-varying system consisting of continuous phases and state-triggered jumps. A continuous control law was derived

to provably stabilize the system during the continuous phases. Lyapunov-based stability analysis was performed to derive sufficient conditions that can be used to directly guide the controller design for provably stabilizing the overall hybrid, time-varying control system. MATLAB and PyBullet simulations, as well as experiments on a physical quadrupedal robot and a pitching treadmill, were performed to validate the proposed control approach. The validation results demonstrated the effectiveness of the proposed approach in realizing stable quadrupedal locomotion on dynamic rigid platforms even in the presence of moderate levels of uncertainties.

REFERENCES

[1] M. Hutter *et al.*, "Anymal-a highly mobile and dynamic quadrupedal robot," in *Proc. IEEE/RSJ Int. Conf. Intell. Robot. Syst.*, 2016, pp. 38–44.

[2] M. Raibert, K. Blankespoor, G. Nelson, and R. Playter, "Bigdog, the rough-terrain quadruped robot," *Proc. Int. Federation Autom. Control*, vol. 41, no. 2, pp. 10822–10825, 2008.

[3] S. Galeani, L. Menini, and A. Potini, "Robust trajectory tracking for a class of hybrid systems: An internal model principle approach," *IEEE Trans. Autom. Control*, vol. 57, no. 2, pp. 344–359, Feb. 2011.

[4] J. B. Biemond, N. van de Wouw, W. P. M. H. Heemels, and H. Nijmeijer, "Tracking control for hybrid systems with state-triggered jumps," *IEEE Trans. Autom. Control*, vol. 58, no. 4, pp. 876–890, Apr. 2012.

[5] F. Forni, A. R. Teel, and L. Zaccarian, "Follow the bouncing ball: Global results on tracking and state estimation with impacts," *IEEE Trans. Autom. Control*, vol. 58, no. 6, pp. 1470–1485, Jun. 2013.

[6] S. Kajita *et al.*, "Biped walking pattern generation by using preview control of zero-moment point," in *Proc. IEEE Int. Conf. Robot. Autom.*, 2003, vol. 2, pp. 1620–1626.

[7] E. R. Westervelt, J. W. Grizzle, C. Chevallereau, J. H. Choi, and B. Morris, *Feedback Control of Dynamic Bipedal Robot Locomotion*, vol. 28. Boca Raton, FL, USA: CRC Press, 2007.

[8] M. A. Sharbafi, M. J. Yazdanpanah, M. N. Ahmadabadi, and A. Seyfarth, "Parallel compliance design for increasing robustness and efficiency in legged locomotion—Proof of concept," *IEEE/ASME Trans. Mechatron.*, vol. 24, no. 4, pp. 1541–1552, Aug. 2019.

[9] A. Mazumdar *et al.*, "Parallel elastic elements improve energy efficiency on the STEPPR bipedal walking robot," *IEEE/ASME Trans. Mechatron.*, vol. 22, no. 2, pp. 898–908, Apr. 2017.

[10] F. Guenther, H. Q. Vu, and F. Iida, "Improving legged robot hopping by using coupling-based series elastic actuation," *IEEE/ASME Trans. Mechatron.*, vol. 24, no. 2, pp. 413–423, Apr. 2019.

[11] X. Liu, A. Rossi, and I. Poulakakis, "A switchable parallel elastic actuator and its application to leg design for running robots," *IEEE/ASME Trans. Mechatron.*, vol. 23, no. 6, pp. 2681–2692, Dec. 2018.

[12] B. Zhong, S. Zhang, M. Xu, Y. Zhou, T. Fang, and W. Li, "On a CPG-based hexapod robot: AmphiHex-II with variable stiffness legs," *IEEE/ASME Trans. Mechatron.*, vol. 23, no. 2, pp. 542–551, Apr. 2018.

[13] C. Li, T. Zhang, and D. I. Goldman, "A terradynamics of legged locomotion on granular media," *Science*, vol. 339, no. 6126, pp. 1408–1412, 2013.

[14] J. Aguilar and D. I. Goldman, "Robophysical study of jumping dynamics on granular media," *Nat. Phys.*, vol. 12, no. 3, pp. 278–283, 2016.

[15] C. M. Hubicki, J. J. Aguilar, D. I. Goldman, and A. D. Ames, "Tractable terrain-aware motion planning on granular media: an impulsive jumping study," in *Proc. IEEE/RSJ Int. Conf. Intell. Robot. Syst.*, 2016, pp. 3887–3892.

[16] X. Xiong, A. D. Ames, and D. I. Goldman, "A stability region criterion for flat-footed bipedal walking on deformable granular terrain," in *Proc. IEEE/RSJ Int. Conf. Intell. Robot. Syst.*, 2017, pp. 4552–4559.

[17] B. Henze, R. Balachandran, M. Roa-Garzón, C. Ott, and A. Albu-Schäffer, "Passivity analysis and control of humanoid robots on movable ground," *IEEE Robot. Autom. Lett.*, vol. 3, no. 4, pp. 3457–3464, Oct. 2018.

[18] J. Englsberger, G. Mesesan, C. Ott, and A. Albu-Schäffer, "DCM-based gait generation for walking on moving support surfaces," in *Proc. IEEE-RAS Int. Conf. Humanoid Robot.*, 2018, pp. 1–8.

[19] Y. Gu, B. Yao, and G. Lee, "Exponential stabilization of fully actuated planar bipedal robotic walking with global position tracking capabilities," *J. Dyn. Syst. Meas. Control*, vol. 140, no. 5, 2018.

[20] *Robot Dynamics Lecture Notes*, ETH Zürich, Robotic Systems Lab, Zürich, Switzerland, 2020. [Online]. Available: https://rsl.ethz.ch/education-students/lectures/robotdynamics.html

[21] H. K. Khalil, *Nonlinear Systems*. Englewood Cliffs, NJ, USA: Prentice-Hall, 1996.

[22] M. S. Branicky, "Multiple Lyapunov functions and other analysis tools for switched and hybrid systems," *IEEE Trans. Autom. Control*, vol. 43, no. 4, pp. 475–482, Apr. 1998.

[23] C. S. Chaney and K. I. Matveev, "Modeling of steady motion and vertical-plane dynamics of a tunnel hull," *Int. J. Nav. Architec. Oce. Eng.*, vol. 6, no. 2, pp. 323–332, 2014.

[24] P. Simeonov, *Impulsive Differential Equations: Periodic Solutions and Applications*. Evanston, IL, USA: Routledge, 2017.

[25] E. Coumans, "Bullet physics simulation," in *Proc. ACM SIGGRAPH*, 2015, pp. 1–1.

[26] "Motek M-Gait." [Online]. Available: https://summitmedsci.co.uk/products/motek-mgait/. Accessed: Nov. 28, 2019.

[27] "Unitree robotics." [Online]. Available: http://www.unitree.cc/product/. Accessed: Nov. 28, 2019.

[28] M. Bloesch, M. Hutter, M. A. Hoepflinger, S. Leutenegger, C. Gehring, C. D. Remy, and R. Siegwart, "State estimation for legged robots-consistent fusion of leg kinematics and IMU," *Robot.*, vol. 17, pp. 17–24, 2013.

[29] R. Hartley, M. Ghaffari, R. M. Eustice, and J. W. Grizzle, "Contact-aided invariant extended Kalman filtering for robot state estimation," *Int. J. Robot. Res.*, vol. 39, no. 4, pp. 402–430, 2020.

Yuan Gao received the B.S. degree in mechanical engineering from China Jiliang University, Hangzhou, China, in 2014, and the M.S. degree in mechanical engineering from Arizona State University, Tempe, Arizona, in 2016. He is currently working toward the Ph.D. degree in mechanical engineering with the Department of Mechanical Engineering, University of Massachusetts Lowell, Lowell, MA, USA.

Amir Iqbal received the B.S. degree in aerospace engineering from the Indian Institute of Space Science and Technology, Thiruvananthapuram, India, in 2012. He is currently working toward the Ph.D. degree in mechanical engineering with the Department of Mechanical Engineering, University of Massachusetts Lowell, Lowell, MA, USA, in 2012.

In 2012, he joined the Indian Space Research Organization as a Scientist/Engineer.

Yan Gu received the B.S. degree in mechanical engineering from Zhejiang University, Hangzhou, China, in 2011 and the Ph.D. degree in mechanical engineering from Purdue University, West Lafayette, IN, USA, in 2017.

Since September 2017, she has been an Assistant Professor with the Department of Mechanical Engineering, University of Massachusetts Lowell, Lowell, MA, USA.